Ocean motion on the Yermak Plateau

- tidal and air-ocean interactions

Eli Anne Ersdal

Thesis for the degree of Philosophiae Doctor (PhD)
University of Bergen, Norway
2020

UNIVERSITY OF BERGEN

Ocean motion on the Yermak Plateau

- tidal and air-ocean interactions

Eli Anne Ersdal

Thesis for the degree of Philosophiae Doctor (PhD)
at the University of Bergen

Date of defense: 02.11.2020

Year: 2020

Title: Ocean motion on the Yermak Plateau

Name: Eli Anne Ersdal

Print: Skipnes Kommunikasjon / University of Bergen

Scientific environment

This study is carried out at the University Centre in Svalbard and I have been enrolled at the University of Bergen. The work is supported by the the Norwegian Research Council funded though the project: Remote Sensing of Ocean circulation and Environmental Mass Change (REOCIRC-222696/F5) and I have been enrolled at the ResClim and Chess Research Schools.

Acknowledgements

I would like to thank my family, friends, colleagues, and supervisor Frank Nilsen at UNIS for always supporting me and helping out when needed. A large part of this project has been to successfully complete field work on the Yermak Plateau. This field work would not have been as successful without the great cooperation between the crew on the research vessels Håkon Mosby, Lance and Helmer Hansen, the students on AGF-214, our cruise leader Eva Falck, and the rest of the team, Ragnheid Skogseth, Tor Gammelrød, Steinar Myking, and Marcos Porcires. On land, among others, Marius Jonassen, Emma Bland, Graham Gilbert, Holt Hancock, Anne Mai Ersdal, Eva Falck and Tor Gammeslrød have contributed to improve my English and proving new ideas. I would also like to thank Roshin Ray for answering my questions on the satellite data, and Kjersti Birkeland Daae and Stephan Kral for providing the overleaf templates.

Skiing always makes me happy, so I am grateful to all of you that joined me for trips around Svalbard. When the contract ended and the deportation became real, the five months of skiing with the Ski & Skred team of 2019 gave me energy and motivation to fulfill this long journey. For the last part of the trip, I thank Matthias Forwick for hosting me at the Institute of Geology in Tromsø, Tromsø kommune for its nice public library, and Jofrid Skarðhamar for lending me an office at the Institute for Marine Research.

A special thanks goes to Siiri, Ylva and Bård Helge.

Eli Anne Ersdal

Longyearbyen, 27th of July 2020

Abstract

This study focuses on the tidal and atmospheric dynamics controlling the overflow of warm Atlantic Water, crossing over the Yermak Plateau, which can be seen as a doorstep to the Arctic Ocean. The Arctic conditions are changing due to the general global warming, and in order to make good predictions of the future climate north of Svalbard and further into the Arctic Ocean, a good understating of the dynamics controlling the overflow is essential. The Yermak Plateau is known for enhanced diurnal tides caused by topographically trapped waves (TTW). A numerical shelf model has been set up for the southwestern side of the plateau to investigate when the TTW near the diurnal frequency become resonant with zero group velocity, meaning that the diurnal energy does not radiate out of the region, but will accumulate along the slope. The model inputs are slope steepness, background current and stratification, and the result indicates that the group velocity of the TTW near the diurnal frequency becomes zero when the background current is strong, i.e. during winter. Four moorings have measured ocean currents and ocean bottom pressure (OBP) on top of the plateau and the data revealed significant monthly and fortnight tidal periods during winter. The low-frequency Lunar Monthly, Mm, and the fortnightly, MSf, are astronomically forced, but their potentials are weak, especially the potential of MSf. Therefore, we suggest that the observed enhancement of Mm and MSf on top of the plateau during winter, is caused by an energy contribution from the diurnal tides. The superposition of Mm and MSf have been termed the Nonlinear Yermak Tidal Overflow (NYTO), and reached a maximum speed of 15 cm s^{-1} in February 2016. From December to May, the mean volume transport was 1.1 Sv by the NYTO alone.

The four moorings located on top of the plateau have been set up to target the Svalbard Branch (SB) and the Spitsbergen Polar Current (SPC). After evaluating the tidal

effect on the Atlantic Water flow across the plateau, these ocean data were coupled with high resolution atmospheric hindcast data to get a deeper understanding of the air-ocean dynamics. The volume transports in the SB and the SPC calculated from the OBP data were correlated with the wind stress curl over Svalbard. As a negative wind stress curl is linked to surface water convergence, southerly alongshore winds stress in the Fram Strait will generate onshore Ekman transport resulting in a convergence zone with a negative wind stress curl on the shelf. This effect steepens the sea surface tilt over the slope, accelerating the ocean current along the slope. In the opposite case, a northerly wind stress generates a westward Ekman transport, weakening the sea surface tilt and decreasing the current speed. Satellite altimetry measurements from 1994 to 2018 were included to investigate the interannual and decadal variations of the oceanic flow passing over the plateau. To validate the performance of satellite altimetry in the SB north of Svalbard, the calculated current fluctuation from satellite altimetry were compared with the current fluctuation derived from the OBP data. Satellite altimetry was found to be useful in calculating the volume transports in winter when the water column has constant density. The winter volume transports from 1994 to 2018 were calculated in three sections, the barotropic West Spitsbergen Current (WSC core), the SB, and the Yermak Pass Branch (YPB) with mean values of 1.4 Sv, 1.1 Sv, and 1.4 Sv, respectively. The flow in the WSC core and the SB correlated with each other throughout the winter season and with the southerly wind stress on the West Spitsbergen Shelf. The flow in the YPB correlated with the northerly wind stress on the West Spitsbergen Shelf and were anti-correlated with the WSC core and the SB from March to May.

Outline

This thesis starts with motivation and objectives (Chapter 1), followed an introductory (Chapter 2), a description of data and methods (Chapter 3), introduction of the four scientific papers (Chapter 4), future perspective (Chapter 5), and papers are included in Scientific results (Chapter 6). The four papers are:

1. Ersdal, E. A. and F. and Nilsen. (2020) *Topographically trapped waves along an Arctic continental shelf in resonance with diurnal tidal frequencies*, Submitted to Journal of Geophysical Research: Oceans (Sept 2019) and resubmitted August 2020.

2. Ersdal, E. A., F. Nilsen, and T. Gammelsrød. (2020) *On nonlinearly enhanced low-frequency tides over the Yermak Plateau*, Submitted to Journal of Geophysical Research: Oceans (Sept 2019).

3. Nilsen, F., E. A. Ersdal, and R. Skogseth (2020) *Atlantic- and Arctic Water transport across the Arctic Sill - Variability in the poleward current branches across the Yermak Plateau*, (Manuscript).

4. Ersdal, E. A., F. Nilsen, R. Skogseth, and E. Falck (2020) *Winter volume and heat transport into the Arctic Ocean from 1994 to 2018 calculated from satellite altimetry.*, (Manuscript).

Contents

Chapter 1

Motivation and Objectives

The environmental setting for this PhD work has been the Yermak Plateau northwest of Svalbard. The main goal has been to understand and describe the ocean dynamics and air-ocean interaction influencing the branching and overflow of Atlantic Water across the plateau towards the Arctic Ocean. A good understanding of the processes controlling inflow of the Atlantic Water toward the Arctic Ocean is crucial in order to make predictions of the future climate in region. In this context, theoretical concepts have been combined with in-situ measurements to increase the knowledge. As a part of the project Remote Sensing of Ocean Circulation and Environmental Mass Balance (RE-OCIRC), two years of ocean data have been collected on the Yermak Plateau. These in-situ ocean measurements of hydrography, ocean currents and ocean bottom pressure have been coupled with satellite altimetry, which measure the sea level anomaly. To our knowledge, this is the first time satellite altimetry has been used to calculate the volume transport in the Svalbard Branch, and therefore, the ocean measurements have also been used to evaluate their performance north of Svalbard.

The main questions addressed during this work are:

- How do meso-scale vortices influence the tidal flow? (**Paper I**)
- How and when do tidal dynamics affect the Atlantic Water overflow on the Yermak Plateau? (**Paper I** and **II**)
- Can satellite altimetry combined with in-situ data be used to estimate the volume and heat transport in the Svalbard Branch? (**Paper III** and **IV**)
- How do the air-sea forcing mechanisms influence the volume transport into the

Arctic Ocean? (**Paper III** and **IV**)

Chapter 2

Background and theory

The global climate is changing due to the atmospheric warming caused by the anthropogenic emissions of CO_2. Since the industrial revolution, the mean global atmospheric temperature has increased about 1 degree, with warming rates in the Arctic roughly double than the to global trend (*IPCC*, 2018; *Pörtner et al.*, 2019). The warming around Svalbard is higher still, even when compared with enhanced warming in other Arctic locations. Over the past decades, from 1971 to 2017, the mean atmospheric temperature in the archipelago has increased between 3 to 5°C (*Hanssen-Bauer et al.*, 2019). Moreover, *Wickström et al.* (2019) have shown that the storm tracks in the Svalbard region have shifted over the last two decades. In winter, the cyclones travel farther north, transporting warm, moist maritime air and precipitation into the region. These winter storms entering the Fram Strait have potentially very damaging short-term effects on the sea ice cover north of Svalbard (*Graham et al.*, 2019). However, the sea ice is also affected from below. *Onarheim et al.* (2014) showed the sea ice concentration north of Svalbard has declined with 10 % per decade since 1979. They linked this sea ice loss to a steady warming of the Atlantic Water north of Svalbard (*Beszczynska-Möller et al.*, 2012; *Onarheim et al.*, 2014; *Piechura and Walczowski*, 2009; *Schauer et al.*, 2004; *Skogseth et al.*, 2020). Further into the Eurasian Basin, *Polyakov et al.* (2017) report on a shoaling of the Atlantic Intermediate Water. The shoaling is primarily caused by a warming of the Atlantic Water, which again weakens the stratification and increases the ventilation, resulting in a thinner sea ice cover. Earlier this "Atlantification" took place in the western Eurasian Basin located north of Svalbard, but over the last two decades this process is also seen in the eastern part of the Eurasian Basin. With this new regime,

the sea ice is no longer protected from the warm Atlantic Water by a strong stratification, and the inflow of Atlantic Water will play a larger role for the sea ice also farther into the Arctic Ocean.

2.1 The Fram Strait – the gateway to the Arctic Ocean

The Atlantic Water originates in the Gulf of Mexico and large wind systems transports the water across the Atlantic Ocean, where a fraction enters the Norwegian Sea. Once in the Norwegian Sea, the main flow of Atlantic Water becomes the Norwegian Atlantic Current which follow two main paths. To the east, the slope current is steered by the slope of the continental shelf (Figure 2.1). To the west, a frontal jet exists on the density front (*Orvik and Niiler*, 2002), guided by the Vøring Plateau (*Nilsen and Nilsen*, 2007), and farther north this frontal branch follows the Mohn and Knipowich Ridges (*Walczowski and Piechura*, 2006). At around 77°N, the two branches begin to

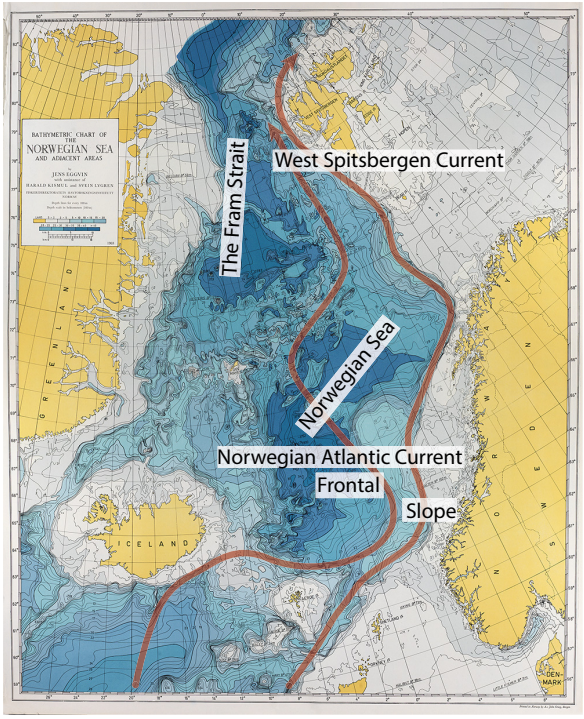

Figure 2.1: The bathymetry map of the Norwegian Sea was originally published by the Institute of Marine Research. The current arrows and the corresponding names have been added for this illustration. The two branches from the Norwegian Atlantic Current placed on top of the bathymetry is roughly redrawn from Figure 1 in Orvik and Niiler (2002). The slope current is seen to the east and the frontal jet to the west.

reconverge just west of Spitsbergen.

The Fram Strait located between Greenland and Spitsbergen is the deepest oceanic entrance into the Arctic Ocean (Figure 2.2). Here, the Norwegian Atlantic Current continues as the West Spitsbergen Current (WSC). The inner slope branch, guided by the steep continental shelf, has a barotropic and a baroclinic component drawn as two red arrows close to west coast of Spitsbergen in Figure 2.2. The barotropic component flows on the shallower side of the 1000 m isobath and its strength is controlled by the sea surface tilt (*Teigen et al.*, 2010). The baroclinic component is located farther west between the 1000 m isobath and the 2400 m isobath and is driven by horizontal density differences (*Gascard et al.*, 1995; *Teigen et al.*, 2011). Hereafter in this thesis, the barotropic component will be referred to as the WSC core and the baroclinic component as the WSC offshore branch, following *Beszczynska-Möller et al.* (2012).

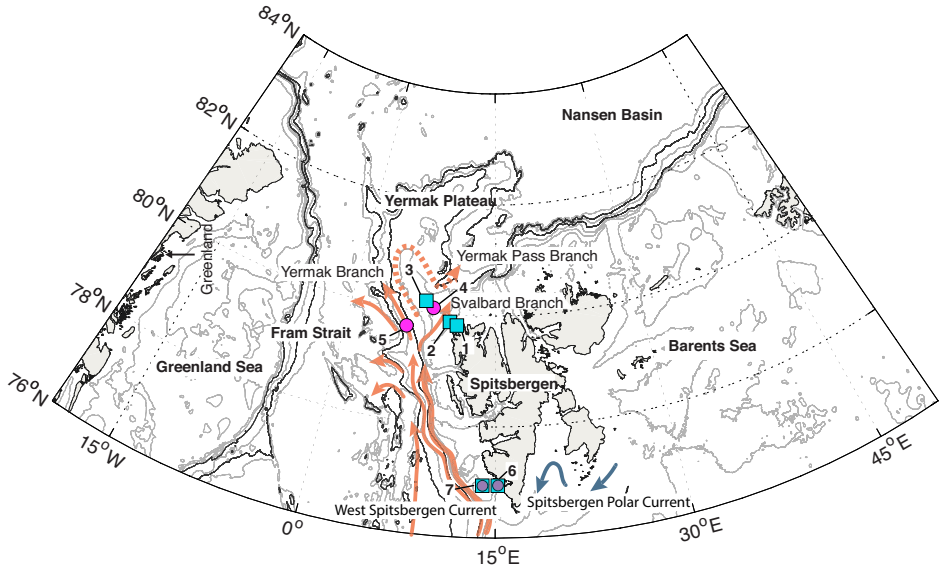

*Figure 2.2: Map showing the current system is the eastern Fram Strait, which is located between Greenland and Svalbard. Three branches of the West Spitsbergen Current (WSC) are drawn as red arrows, from the west, the extension of the frontal jet, the offshore branch, and the core of the WSC. Close to the Yermak Plateau, the WSC splits into the Yermak Branch (YB), the Yermak Pass Branch (YPB) and the Svalbard Branch (SB). The Spitsbergen Polar Current (SPC) is drawn close to the coast in blue (Helland-Hansen and Nansen, 1909). In addition, the seven moorings, numbered 1 to 7 used in this work are marked with turquoise squares and pink circles. More details on moorings are given in Table 3.1 (**Paper II**).*

The WSC flows northwards along complex and rough topography, which creates unstable eddies spinning off westwards. The eddy activity intensifies in winter when the WSC current is strong (*Bashmachnikov et al.*, 2020; *Hattermann et al.*, 2016; *Teigen*

et al., 2010, 2011; *von Appen et al.*, 2016). Consequently, a large fraction of the Atlantic Water is recirculated in the Fram Strait (*Bourke et al.*, 1988; *Gammelsrød and Rudels*, 1983; *Gascard et al.*, 1995; *Teigen et al.*, 2011). *Marnela et al.* (2013) showed that about 50 % of the AW is recirculated between 76 and 81°N.

2.1.1 The Yermak Plateau – the doorstep to the Arctic Ocean

At the northwest corner of Spitsbergen, the isobaths and currents diverge when approaching the Yermak Plateau's considerable vertical relief. Here, steep marginal slopes plunge from the plateau summit at 600 m to depth of 4000 m, forcing Atlantic Water in the WSC to diverge and either traverse the broad, shallower summit or skirt to plateau margins to enter the Arctic Ocean. The WSC core extends as the Svalbard Branch (SB) across the inner part of the plateau on the shallower side of the 500 m isobath (*Aagaard et al.*, 1987). The offshore branch following deeper isobaths is guided along the southwestern side, and the classical description is that the current continues around the rim as the Yermak Branch (YB) (*Manley et al.*, 1992; *Rudels et al.*, 2000). However, the fate of this branch is not fully understood and *Gascard et al.* (1995) and *Koenig et al.* (2017) have suggested a new path over the central plateau, the Yermak Pass Branch (YPB). This branch is present during winter and is steered roughly by the 700 m isobath. The current measurement presented by *Koenig et al.* (2017) showed that the YPB sends pulses of Atlantic Water across the Yermak Plateau. The observed pulses have a period of 5 to 15 days and 1 to 2 months.

Topographically trapped waves around the Yermak Plateau close to the diurnal frequency

The Yermak Plateau is known for strong tidal currents, mixing the warm Atlantic Water and help maintain ice-free conditions (*Fer et al.*, 2010, 2015). The diurnal tides over the plateau are unusually strong, and periodically they exceed the strength of the semidiurnal currents (*Hunkins*, 1986; *Kowalik*, 1994; *Padman et al.*, 1992). *Cartwright* (1969) was probably the first to address topgraphically enhanced diurnal tides, observed over Rockall Bank west of Scotland. Most subsequent observations of topographically enhanced tides are from higher latitudes in both the northern and southern hemisphere (*Foldvik et al.*, 1990; *Hunkins*, 1986; *Huthnance*, 1978; *Middletton et al.*, 1987; *Padman et al.*, 1992; *Semper and Darelius*, 2017; *Skarðhamar et al.*, 2015). On

the Yermak Plateau, *Hunkins* (1986) was the first to report on the unusually strong diurnal tides based on current measurements made from a drifting ice floe. He observed the diurnal tides were particularly strong at the shelf break, and the oscillating current was oriented across-slope, in contrast to the semi-diurnal tides oriented along-slope. Based on these findings he suggested that the diurnal frequency was enhanced by near-resonate vorticity waves close to the diurnal frequency. A sub-inertial tidal frequency, where the inertial frequency (f) at a specific latitude, is larger than the tidal frequency (ω), has the potential to be trapped by the topography (*Foldvik et al.*, 1990). In the northern hemisphere, the critical latitude (where $f = \omega$) occurs near 30°N for the diurnal tides (*Furevik and Foldvik*, 1996). Later *Padman et al.* (1992) gathered available observational data and included a simple shelf model. Using the model, they investigated how altering the steepness of the slope shifts the frequency at which the group velocity, c_g, becomes zero. When c_g is zero the energy does not propagate out of the area, but instead accumulating at the slope. From the model simulation, they suggested that near-resonate topographic shelf waves with $c_g = 0$ close to the diurnal frequencies, K1 and O1 can explain the enhanced diurnal tides. Figure 2.3 shows an example of the structure of topographically trapped waves (TTW) with frequency near the diurnal K1 component. Here, the continental shelf wave model (*Brink*, 2006) has been used along the southwestern slope of the Yermak Plateau to test under what conditions the group velocity becomes zero. (The example shown is from **Paper I**).

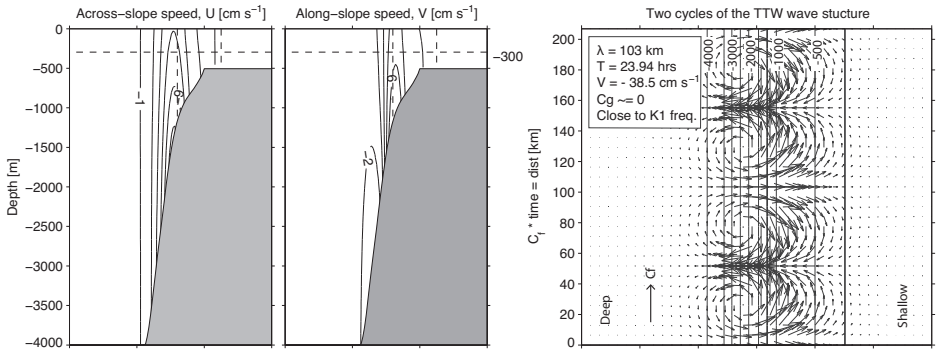

*Figure 2.3: The structure of a TTW with zero group velocity near the diurnal K1 frequency has been modelled along the southwestern side of the Yermak Plateau (**Paper I**). The vertical structure of the vortex with the eastward component is seen in a) and the northward component is seen in b). The horizontal structure of two cycles seen from above is plotted in c).*

Tides

Tidal currents can be seen as the superposition of several hundred constituents and the tidal periods range from a few hours to more than 20 000 years. Out of these are 37 purely astronomical, while the rest are termed the shallow-water constituents generated through nonlinear tidal dynamics (*Parker*, 2007; *Pawlowicz et al.*, 2002). Table 2.1 shows the period, the frequency, the critical latitude, and possible nonlinear connections for twelve astronomical tidal constituents, with periods ranging from 12.42 hours to 182.6 days. The tidal constituents are sorted by their tidal potential within the three species: semidiurnal, diurnal and low-frequency tides.

Table 2.1: Tidal constituents with their period in days, frequency, critical latitude and the possible nonlinear connections, found by summing or subtracting the frequencies.

Constituents		Period [days]	Frequency ω [hr $^{-1}$]	Critical latitude, ϕ	Nonlinear connections
Semi-diurnal					
M2	Principal lunar	0.518	$8.0511 \cdot 10^{-2}$	74°28.50′	K1 + O1
S2	Principal solar	0.500	$8.3333 \cdot 10^{-2}$	85°46.62′	K1 + P1
N2	Principal lunar elliptic	0.527	$7.8992 \cdot 10^{-2}$	70°58.93′	K1 + Q1
K2	Sun-Moon angle	0.499	$8.3662 \cdot 10^{-2}$	90°00.00′	
Diurnal					
K1	Sun-Moon angle	0.998	$3.1781 \cdot 10^{-2}$	30°00.00′	M2 - O1
O1	Principal lunar declination	1.076	$3.8731 \cdot 10^{-2}$	27°36.82′	M2 - K1
P1	Principal solar declination	1.003	$4.1553 \cdot 10^{-2}$	29°49.20′	S2 - K1
Q1	Principal lunar declinational	1.119	$3.7218 \cdot 10^{-2}$	26°26.97′	N2 - K1
Low-frequency tides					
Mf	Lunisolar fortnightly	13.66	$3.0501 \cdot 10^{-3}$	02°05.51′	K2 - M2, K1 - O1
Mm	Lunar monthly	27.55	$1.5122 \cdot 10^{-3}$	01°02.21′	M2 - N2, O1 - Q1
SSa	Semi solar annual	182.6	$2.2816 \cdot 10^{-4}$	00°09.39′	K1 - P1, K2 - S2
MSf	Lunisolar synodic	14.76	$2.8219 \cdot 10^{-3}$	01°56.12′	S2 - M2, P1 - O1

Critical latitude ($\omega = f$, $f = 2\Omega sin\phi$, ϕ = latitude)

Generally, the most energetic and recognizable tides are the semidiurnal M2 and S2 tides with periods around 12 hours. The ocean tides are forced by the gravitational pull between the earth and the moon as well as the earth and the sun (*Parker*, 2007). The astronomical tidal forcing is changing as the earth, the moon and the sun continuously are moving relative to each other. The moon creates two tidal bulges on the earth, one pointing towards the moon and the second pointing away from the moon. On a rotating earth, an observer will see this as two high tides, and two low tides per day. The sun also creates two tidal bulges on the earth, but they are smaller than those forced by the moon. The diurnal tides have a period of around 24 hours and can be seen as the inequality between the two daily high tides (e.g. the semidiurnal M2). An observant

observer can see that over one day, one high tide is stronger than the following high tide. This inequality is caused by the inclination between the earth's equatorial plane and the moon (and sun). The diurnal tides are strongest around solstice when the inclination between the earth's equatorial plane and the sun is at its maximum, and weakest around the equinoxes when the sun is above the equator (*Parker*, 2007).

The assumption of tides with linear dynamics is adequate for the deep ocean, but nonlinearity may become important in shallower areas and over continental shelves (*Le Provost*, 1991; *Parker*, 1991). The shallow-water tidal constituents are nonlinear and arise when the astronomical tides interact with shallow and complex bathymetry. The most common examples are from narrow sounds or estuaries where sub-harmonics and compound tides (e.g. M4 or MS4) can be generated from, and at the expense of, the astronomical constituents M2 and S2. The semidiurnal M2 and S2 can also feed low-frequency compound tides such as the fortnightly MSf with a period of 14.75 days. The compound tides are linked through the frequencies of the two tidal constituents interacting, where $\omega(\mathrm{MSf}) = \omega(\mathrm{S2}) - \omega(\mathrm{M2})$. The significance of MSf, which has a weak tidal potential, is an especially strong indicator that nonlinear tidal dynamics are important (*Wuncsh*, 1967). More examples on nonlinear connections are given in Table 2.1 and in *Parker* (1991). The low-frequency tides shown in Table 2.1 are astronomically driven, but their response is relatively weak. However, in regions where nonlinear tidal dynamics are important, these long-period tides can receive energy contributions, e.g. from the energetic M2 through nonlinear processes (*Kantha et al.*, 1998). The Yermak region is known for enhanced diurnal tides generated by TTW, existing along the steep continental slope surrounding the plateau, and it is also possible that MSf receive energy from the diurnal tidal band, as $\omega(\mathrm{MSf}) = \omega(\mathrm{P1}) - \omega(\mathrm{O1})$.

The Yermak Plateau is a shallow topographical obstacle, which the WSC carrying Atlantic Water northwards must overcome in order to enter the Arctic Ocean. The region is already known as a special place regarding tidal dynamics, and hence, it is likely a region where nonlinear tidal dynamics can become important. The effect of the strong tides is that the warm Atlantic Water passing by, is mixed up to the surface, melting the sea ice and affecting the dynamics at the air-ocean interface (*Fer et al.*, 2010, 2015; *Sirevaag and Fer*, 2009). The strong tidal mixing makes the area attractive

to marine life, and in the early days the southern part of the plateau was referred to as Whaler's Bay (*Onarheim et al.*, 2014). Is it also possible that the tides in the region influence the inflow of Atlantic water into the Arctic Ocean? *Koenig et al.* (2017) have already reported that the warm Atlantic Water in the Yermak Pass Branch is transported across the plateau in pulses.

2.1.2 Using satellite altimetry to investigate long term variations

The density difference between the water masses is crucial to keep the global current system running, but on decadal, interannual and seasonal time scales, the wind forcing will regulate the intensity of the regional current (*Bringedal et al.*, 2018). The radar satellite altimetry data date back to the early 90s and can provide information about long term variations. In the Norwegian Sea, *Mork and Skagseth* (2010) have combined satellite altimetry and hydrography to investigate long term variability in the Norwegian Atlantic current. In another study using satellite altimetry, *Chafik et al.* (2015) coupled the flow in the Norwegian Atlantic Current with inflow into the Barents Sea and the Fram Strait. They included atmospheric forcing in their study, and found that the flow in the Norwegian Atlantic Current and the inflow into the Barents Sea were linked to the atmospheric forcing in the Nordic Seas, while the flow in the Fram Strait responded to the regional wind forcing over Svalbard and in the northern Barents Sea. Traditionally, satellite altimetry has not been used this far north, but in addition to *Chafik et al.* (2015), *von Appen et al.* (2016) have used satellite altimetry in the Fram Strait to investigate eddy kinetic energy. Recently, *Bashmachnikov et al.* (2020) investigated eddies in the Fram Strait and Greenland Sea by combing satellite altimetry, synthetic-aperture radar (SAR), and ocean numerical models. With this approach they detected large mesoscale eddies with radii of 30-50 km. The eddies were primarily present in winter and the distribution between cyclonic and anticyclonic eddies was equal.

An overly smoothed geoid, which results in a poor presentation of the boundary currents in coastal areas (*Rio et al.*, 2018) has been a problem with satellite altimetry. To improve the geoid, GOCE (Gravity Field and Steady-State Ocean Circulation Explorer), and the twin satellites GRACE (Gravity Recovery and Climate Experiment)

were launched into lower orbits to measure the gravity field of the earth (*Rio et al.*, 2013). The GOCE mission lasted from 2009 to 2013 and the GRACE mission from 2002-2017, and the follower GRACE_FO was launched in 2018. By including these satellite data, a new Mean Dynamic Topography (MDT) with higher resolution (1/8°) has been released by AVISO. This MDT has a much better representation of boundary currents such as the WSC and the SB.

Chapter 3

Data and methods

3.1 Overview of the data sets

3.1.1 The REOCIRC mooring program (2014 to 2016)

As a part of the REOCIRC field campaign, four moorings were deployed in August 2014 on the Yermak Plateau with the help from the crew at R/V Håkon Mosby (Figure 2.2). One year later, the moorings were recovered and re-deployed, and the final recovery occurred in August 2016. Three of these moorings, YP1-3, from hereafter denoted as Mo. 1 to 3 (Figure 2.2 and Table 3.1), measured the ocean bottom pressure (OBP), and Y-Sh(allow) (Mo. 4) was equipped to measure the ocean current and hydrography. See Table 3.1 for more details on the mooring set up. During the same field campain, but financed by the AWAKE project, two additional OBP moorings equipped with a current meter, were deployed outside Hornsund (Mo. 6 and 7). During September 2015, another mooring, Y-De(ep), (Mo. 5) was deployed with K/V Svalbard (the UNDER-ICE project) at the southwestern slope of the Yermak Plateau and 11 months of data from one current meter are included in this study. All data have been published in the Norwegian Centre for Research Data (*Falck*, 2019; *Nilsen*, 2019).

3.1.2 Satellite altimetry

The satellite altimetry product is produced and provided by the Copernicus Marine Environment Monitoring Service (CMEMS). Both the along-track and gridded product with a resolution of 1/4° have been downloaded. This gridded product provides several

Table 3.1: Description of the seven moorings. The numbers, 1 to 7, show the positions of the seven moorings the map in Figure 2.2

Mo. number	Mooring	Latitude	Longitude	Depth [m]	Parameter
1	YP1	79° 47.958′	010° 44.75′	27 / 29	OBP, S x 1, T x 2
2	YP2	79° 50.442′	010° 29.60′	110 / 110	OBP, S x 1, T x 3
3	YP3	80° 10.467′	008° 08.71′	550 / 550	OBP S x 1, T x 3
4	Y-Sh	80° 07.100′	008° 32.04′	512 / 515	V x 3, S x 3, T x 15
5	Y-De	79° 44.093′	005° 56.33′	1207	V x 1
6	HO1	77° 00.270′	015° 11.38′	38 / 38	OBP, V x 1, S x 1, T x 2
7	HO2	76° 57.537′	014° 04.21′	86 / 88	OBP, V x 1, S x 1, T x 2

Measuring periods:
YP1-3, Y-Sh: 28.08.2014 - 27.08.2015 and 28.08.2015 - 13.08.2016 (2 yr)
HO1-2: OBP from 01.09.2014 - 25.08.2015 and 02.09.2015 - 18.08.2016 (2 yr)
HO1-2: Current meters from 02.09.2015 - 18.08.2016 (2 yr)
Y-De: 11.09.2014 - 13.08.2015 (11 months)
OBP − Ocean bottom pressure measured 1 m above bottom.
V − Current velocity, S − Salinity, T − Temperature

parameters such as the mean dynamic topography (MDT) and the absolute dynamic topography (ADT), but here only the sea level anomaly (SLA) has been utilized. The ADT is the SLA relative to the MDT (Figure 3.1), and instead of using the MDT CNES-CLS13 (1/4°) provided by CMEMS, the MDT CNES-CLS18 from AVISO (Archiving, Validation and Interpretation of Satellite Oceanographic data) with higher resolution of 1/8° has been used. The SLA data with 1/4° resolution have been linearly interpolated to match the high resolution MDT. For more detailed information about the satellite data, see **Paper III** and **IV**.

3.1.3 Hydrographic data

Data from the UNIS hydrographic data base have been used in **Paper II**, **III** and **IV**. The database have published in (*Skogseth et al.*, 2019) and a more detailed description of the data is given in (*Skogseth et al.*, 2020).

3.1.4 Atmospheric data

The NORA10 data set is a high resolution (10 x 10 km) wind and wave hindcast database which is based on a dynamical downscaling of ERA-40 and operational analyses from ECMWF. The data set covers Svalbard, the eastern Fram Strait, and the Barents Sea. The data are provided by the Norwegian Meteorological Institute (https://thredds.met.no/thredds/projects.html) and are described in *Reistad et al.* (2011, 2015). The data are used in **Paper III** and **IV**.

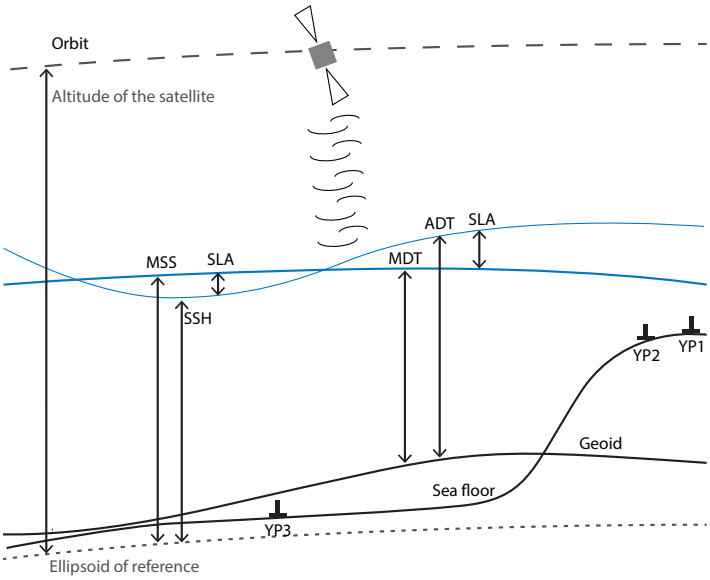

*Figure 3.1: The illustration has been redrawn from the homepage: https://duacs.cls.fr/. The Mean Sea Surface (MSS) and the Sea Surface Height (SSH) relates to the ellipsoid of reference, while the Mean Dynamic Topography (MDT) and the Absolute Dynamic Topography (ADT) relate to the geoid. The Sea Level Anomaly (SLA) is the deviation from the mean. The three moorings YP1-3 have been included in the drawing (**Paper III**).*

3.1.5 Sea Ice concentration

The Global Sea Ice Concentration climate data record (SMMR/SSMI/SSMIS) by EUMETSAT OSI SAF (*Lavergne et al.*, 2019) has been downloaded from osisaf.met.no. Climate data records are made for 1978 to 2015 (*OSISAF*, 2017), while a Global Sea Ice Concentration interim climate data record, release 2 covers from 2016 up until present minus 16 days (acronym: GBL SICO ICDR 2). The dataset has a horizontal grid resolution of 25 x 25 km. The data are used in **Paper I** and **IV**.

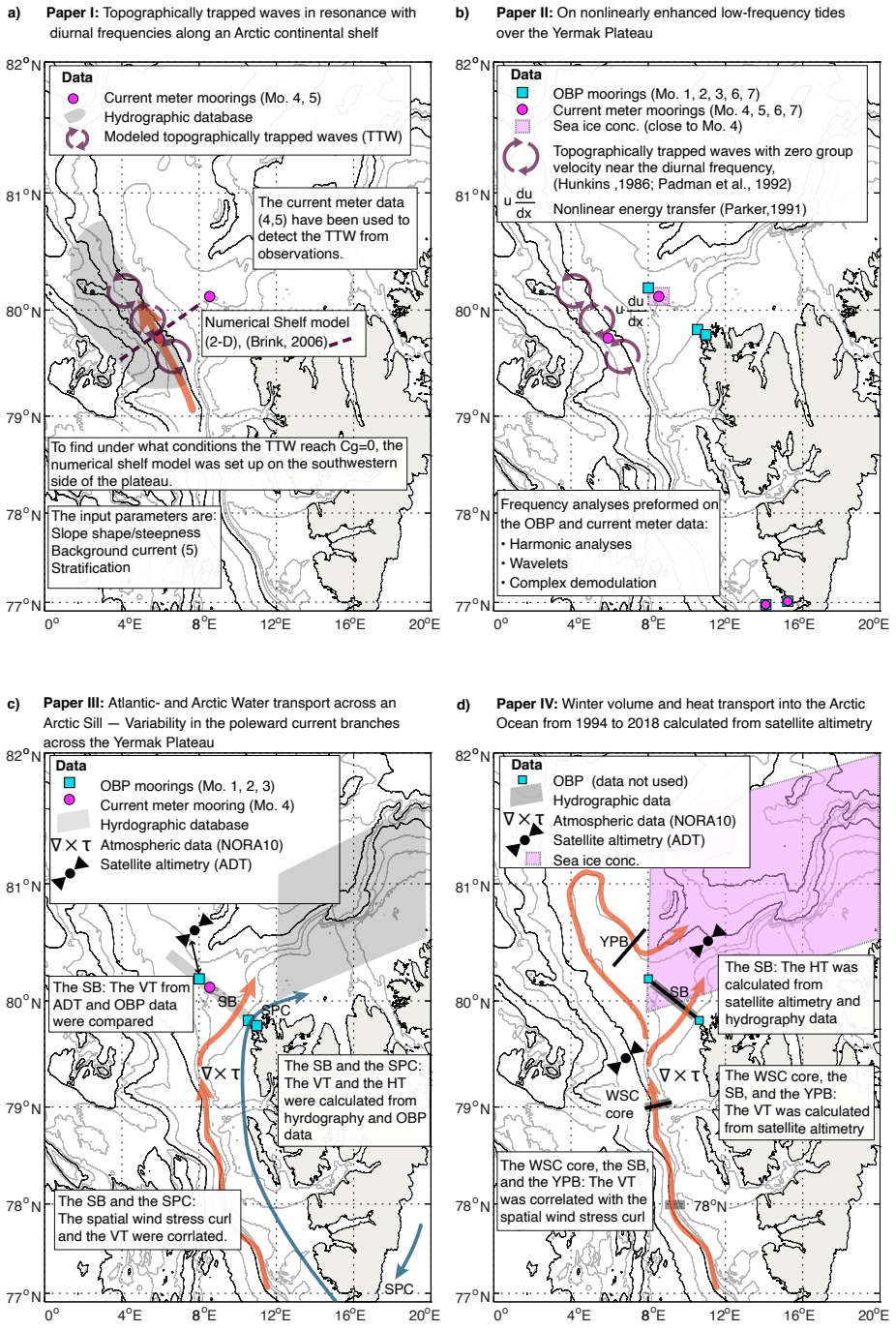

Figure 3.2: The figure show four maps over Spitsbergen, the eastern Fram strait and the southern Yermak Plateau, each describing one of the ***Papers I-IV****. The type of data with the corresponding positions are shown on the map. The mooring numbers (Mo. 1 to 7) refer to Figure 2.2 and Table 3.1. A very brief description of the methods and what has been investigated are also included in the plots. In c) and d), the volume and heat transport have been abbreviated as VT and HT, respectively.*

Figure 3.2 gives a schematic overview of the data which has been used in the four papers. Each subplot also contains a brief description about the application of the data.

3.2 The REOCIRC field campaign

A large part of this thesis work has been used to plan and execute the field work on the Yermak Plateau. This region is located in the marginal ice zone, and therefore difficult to access for large portions of the year. As a result, there are very few long time series published from the region. *Morison* (1991) has published three years of ocean bottom pressure data from 1982 to 1985 and *Koenig et al.* (2017) has published a one year long ADCP (Acoustic Doppler Current Profiler) record from 2007 to 2008.

The ocean current can be measured directly with moored current meters or profilers. However, this study has tested out measuring the geostropic current indirectly from paired pressure sensors at the bottom of the sea floor. The two OBP moorings deployed outside Hornsund (HO1−2) and the two inner most moorings on the Yermak Plateau, YP1 and YP2 (Mo. 6 and 7 and 1 and 2) were placed to capture the pressure difference across the SPC (*Helland-Hansen and Nansen*, 1909). YP2 and YP3 (Mo. 2 and 3) were positioned to measure the pressure difference across the Svalbard Branch. From 1982-1985, *Morison* (1991) measured the ocean bottom pressure (OBP) across the SB and we followed his approach and deployed our moorings close to the same positions. This measuring approach was new to us, but with help and guidance from the team at the Applied Physics Lab in Seattle, we created a new mooring design shown in Figure 3.3. The picture shows the new mooring construction, which has been placed on the bottom of the ocean. The Seabird 26plus measuring the pressure is placed inside the small steel cylinder, seen to the left in Figure 3.3. The instrument needs to be kept in a fixed position in order to limit the measuring error and the noise. The acoustic release is attached at the top of the construction and a microcat seabird37 is placed 3 m above the ocean floor. All the five OBP moorings have the same design, however, depending on the depth, one or two Vemco mini logger II measured the temperature higher up in the water column (Table 3.1).

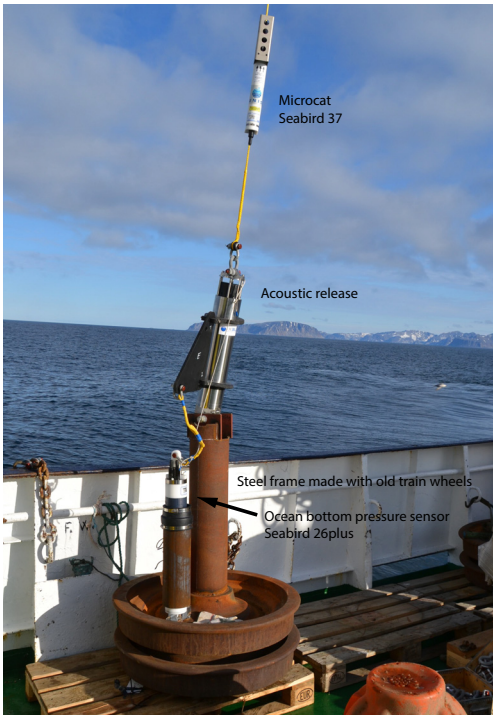

Figure 3.3: The picture shows the new mooring construction that is placed on the bottom of the ocean. The seabird 26plus measuring the pressure is placed inside the small steel cylinder seen to the left. The acoustic release is attached to the top of the construction and a microcat seabird37 is placed 3 m above the ocean floor. Photo: Eli Anne Ersdal.

First, the measured pressure difference can be used to calculate the barotropic competent of the mean geostrophic current variability, v_{bt}, between the two paired moorings:

$$v_{bt} = \frac{1}{f\rho_0}\frac{\partial P}{\partial x} \tag{3.1}$$

here, v_{bt} is the barotropic current speed variation in y-direction, f is the coriolis parameter, ρ_0 is the constant density of sea water, P is the pressure, and x is the distance between two the moorings. This simplified approach (Eqn. 3.1) is based on the assumptions of a flat bottom and constant water density between the paired moorings. In **Paper III** (Figure 3.2c), the volume and the heat transport across the plateau and towards the Arctic Ocean have been calculated using OBP (Mo. 1 to 3 in Table 3.1).

A second motivation for deploying the OBP moorings was to validate the perfor-

mance of satellite altimetry north of Svalbard. To our knowledge, satellite altimetry has not been used to estimate the volume transport at this latitude i.e., in the SB. The OBP sensor measures the changing sea surface elevation from below, while the satellite measures the sea level anomaly (SLA) from above. Figure 3.1 illustrates the satellite orbiting the earth, measuring the distance down to the sea surface with a radar. The main output is SLA relative to the mean sea surface (MSS). However, in order to calculate the geostropic surface current from satellite altimetry, the SLA relative to the MDT is required. Here, we combined the SLA from CMEMS and the last MDT provided by AVISO to calculate the absolute dynamic topography, ADT = SLA + MDT. These two data sets have the same reference period (1993−2012) and are therefore compatible. The ADT maps the highs and lows in the ocean and the gradient can be used to calculate the surface velocity, v_s.

$$v_s = \frac{g}{f}\frac{\partial \eta}{\partial x} = \frac{g}{f}\frac{\partial ADT}{\partial x} \tag{3.2}$$

here v_s is the northward surface current, g, gravity, f the Coriolis parameter, and both η and ADT represent the sea surface elevation. With a well-mixed ocean with constant density ocean, one can assume the barotropic surface current, v_s, equals the barotropic component, v_{bt}, which is constant through the water column. The assumption of a well mixed water column with constant density is a valid assumption on the Yermak Plateau during winter (Figure 3.4), and consequently, the OBP and the SLA variations would be comparable.

After comparing the volume transport in the SB calculated from OBP and altimetry data (**Paper III**, Figure 3.2c), a 24 year long altimetry record was used to estimate the winter volume transport with the SB towards the Arctic Ocean (**Paper IV**, Figure 3.2d).

When AVISO post-processes the satellite altimetry data, the sea level changes from the atmosphere and the tidal elevation are removed. A good result depends on how well the tidal dynamics are represented in the region. A third usage for the OBP data, which often are referred to as tidal gauges, is to perform tidal analyses. Two year long records of the current and the sea level elevation (OBP) are unique, especially in this re-

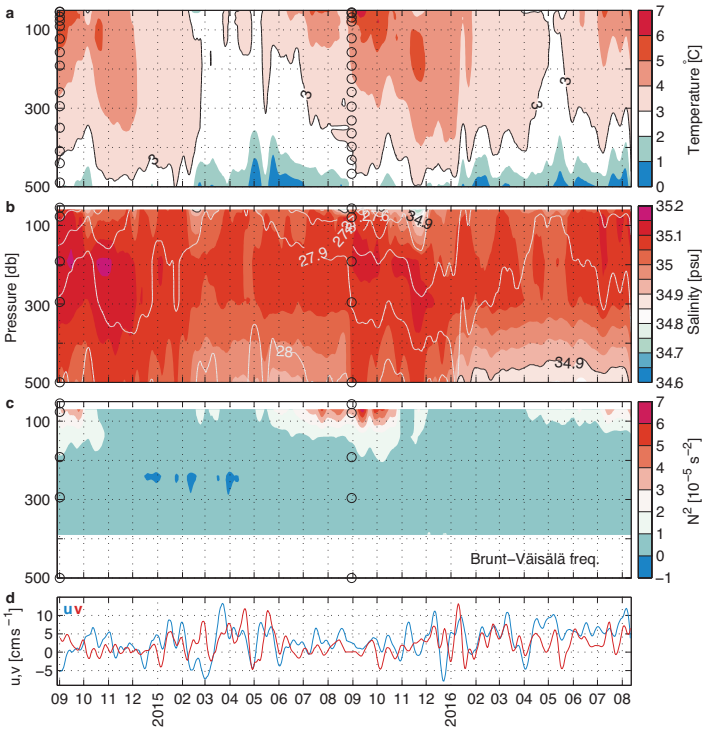

*Figure 3.4: The sea water properties in the water column at Y-Sh from 28.08.2014-11.08.2016 described in Hovmöller diagrams with time along the x-axis. Temperature is shown in the top panel, the salinity and potential density, σ_θ (gray lines) in the second panel and the buoyancy frequency N^2 below. The depths of the instruments are marked with black circles along the y-axis. The conductivity measurement on 500 m is adapted from YP3. The mean vertical current shown at the bottom is calculated from the current meters at 60 m and 500 m. The data are daily means smoothed with a seven days low-pass filter (**Paper III**).*

gion known for complicated tidal dynamics. The tidal elevation and ocean current have been analyzed with harmonic analyses (*Pawlowicz et al.*, 2002). The Yermak Plateau is known for enhanced diurnal tides ($\sim$ 24 hrs), and with these long time series we were able to detect the importance of low-frequency ($\sim$ 14 and 28 days) tidal dynamics on top of the plateau (**Paper II**, Figure 3.2b). For this purpose, we applied wavelets (*Lilly and Olhede*, 2009; *Olhede and Walden*, 2002) and complex demodulation (e.g. *Emery and Thomson* (2001)).

To increase the understanding of when diurnal tides are enhanced and what the most important factors in this enhancement are, we have utilized a simple numerical model for the southwestern slope of the Yermak Plateau. The model set up is described in *Brink* (2006) and the code is run in Matlab. The main input parameters are the slope

steepness, the stratification and the strength of the background current. The model is two-dimensional and the output is the dispersion relation of the vorticity waves that can exist along the slope under given conditions. The in-situ data were used to detect the TTW and the current data from Y-De (Mo. 5) were used as input for the background current. More details on the model set up is give in **Paper I** (Figure 3.2a).

Chapter 4

Main results from the papers

Paper I: **Topographically trapped waves along an Arctic continental shelf in resonance with diurnal tidal frequencies**

Ersdal, E.A., F. Nilsen, Submitted (Sept 2019), re-submitted (August 2020), JGR-Ocean

The main goal of **Paper I** has been to get a better understanding of when the diurnal tides become enhanced along the continental slope of the Yermak Plateau. A simple numerical shelf model has been set up to model the TTW existing along the southwestern side of the Plateau. The model has three main input parameters, the slope steepness and shape, the stratification and the strength of the along-slope current. The output is the dispersion, $\omega(l)$, which relates the wavenumber, l, and the frequency, ω, of the vorticity wave. The aim is to investigate the frequency, and under which conditions the group velocity, c_g, of the TTW becomes zero within the diurnal band, here defined as the Zero Group velocity Frequency (ZGF). See the illustration in Figure 4.1. A favorable slope profile is a prerequisite for the wave to have the potential of being trapped. The slope does not change, but the stratification and current strength change with the seasons. To get a realistic input, we made seasonal stability profiles along the slope from a hydrographical database. The model runs show that the dispersion relation is most sensitive to changes in the stratification along the slope between 500 and 1200 m. At the study area, the seasonal stratification does not change much at these depths. However, the most efficient way to alter the dispersion relation is to change the along slope mean current over this submerges plateau. The model shows that the TTW can exist along the slope all seasons, but mostly with $c_g > 0$ or $c_g < 0$, implying that the en-

Paper I: Topographically trapped waves in resonance with diurnal frequencies along an Arctic continental shelf

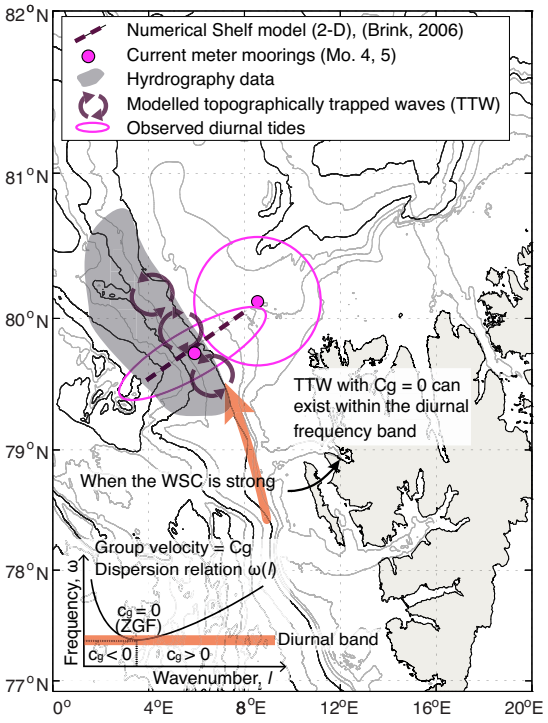

*Figure 4.1: A schematic illustration of the mains findings in **Paper I**.*

ergy radiates out of the area. The main result is that when the current intensifies, the dispersion relation moves to higher frequencies. Now the minimum of the dispersion curve, the ZGF, is placed within the diurnal band. When ZGF is reached, the energy linked to the enhanced frequency will accumulate along the slope. The diurnal constituents with the lowest frequency such as Q1 and O1 become resonant and reach ZGF with a weaker background current, compared to the high frequency K1 and P1 which require higher speed to become resonant with ZGF.

Based on these model results, we suggest that the diurnal tides at the southwestern slope of the Yermak Plateau have the largest potential of enhancement in winter. The enhancement of the lower diurnal frequencies O1 and Q1 is linked to a moderate current strength, hence, O1 and Q1 are probably more frequently enhanced compared to the higher frequencies, K1 and P1.

Paper II: **On nonlinearly enhanced low-frequency tides over the Yermak Plateau.**

Ersdal, E.A., F. Nilsen, and T. Gammelsrød. Submitted (Sept 2019), JGR-Ocean

Two years of OBP measurements and current data on top of the Yermak Plateau show that the fortnightly MSf and monthly Mm tidal periods become significant in winter. The astronomically forcing of the MSf and Mm tidal constituents is weak, and therefore are they not significant in most regions. However, in regions where nonlinear tidal dynamics are important, they can receive an energy contribution from the energetic high frequency tides. In most areas, the energetic, semidiurnal M_2 is a strong candidate, but the Yermak Plateau is known for enhanced diurnal tides, which also can redistribute their energy to other frequencies.

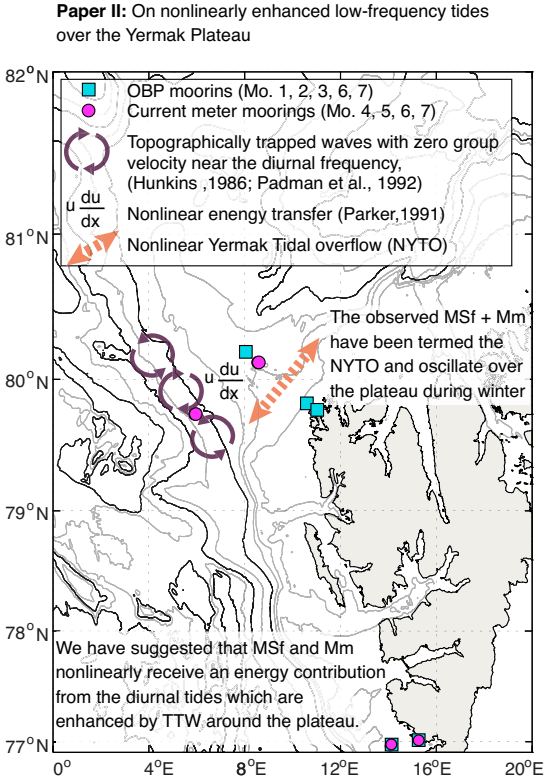

*Figure 4.2: A schematic illustration of the mains findings in **Paper II**.*

In **Paper I**, we find that the TTW become resonant and with zero group velocity (c_g) when the WSC is strong. A strong WSC typically occurs in winter, and this coincides

with the observed enhancement of MSf and Mm. Therefore, we suggest that the excess accumulated diurnal energy generated by the topographically trapped waves with $c_g = 0$, is transferred to Mm and MSf on top of the plateau. The superposition of MSf and Mm sets up a current transporting pulses of Atlantic Water across the plateau. This flow has been termed the Nonlinear Yermak Tidal Overflow (NYTO), see the illustration in Figure 4.2. We estimated the volume transport generated by the NYTO across the plateau to be 1.0 ± 1.3 Sv with a corresponding mean heat flux of 12.3 ± 16.3 TW.

Paper III: **Atlantic- and Arctic Water transport across an Arctic Sill – Interannual variation in the poleward branches across the Yermak Plateau**

Nilsen, F., E.A. Ersdal, and R. Skogseth (Manuscript)

The volume transport fluctuations in the Svalbard Branch (SB) and the Spitsbergen Polar Current (SPC) have been calculated from the paired OBP sensors on the Yermak Plateau (Figure 4.3). From August 2014 to August 2016, the peak-to-peak variation in the Svalbard branch is 4 Sv (1 Sv = 10^6 m^3 s^{-1}) and 0.8 Sv in the SPC. Further, the OBP records have been used to validate how well satellite altimetry performs north of Svalbard. The finding is that OBP data smoothed with a 10-day low-pass filter correlates well with sea level anomalies from satellite altimetry. The correlation coefficient for a 30 day gliding window varies seasonally. However, during the first winter, the mean correlation coefficient was relatively high with r $\sim$0.8 from mid-November through April. The following year was more variable with r $\sim$0.5 from August through June.

The next step was to couple the OBP data with the atmospheric forcing. The tidal signal has been removed from the OBP records, leaving us with the atmospheric forcing on sea surface. The observed atmospheric forcing has been linked to the wind stress curl over Svalbard, which has been calculated from NORA10 hindcast data with a relatively high resolution of 10 x 10 km. The wind stress curl over the Yermak Plateau and also upstream on the shelf west of Spitsbergen correlates with the volume transport in the SB. The NORA10 data also showed that a high spatial resolution is necessary in order to reproduce the Ekman transport generated by the wind stress. The redistribution of the surface water changes the sea surface tilt, which leads to an acceleration or reduction

of the oceanic flow. See the illustration in Figure 4.3.

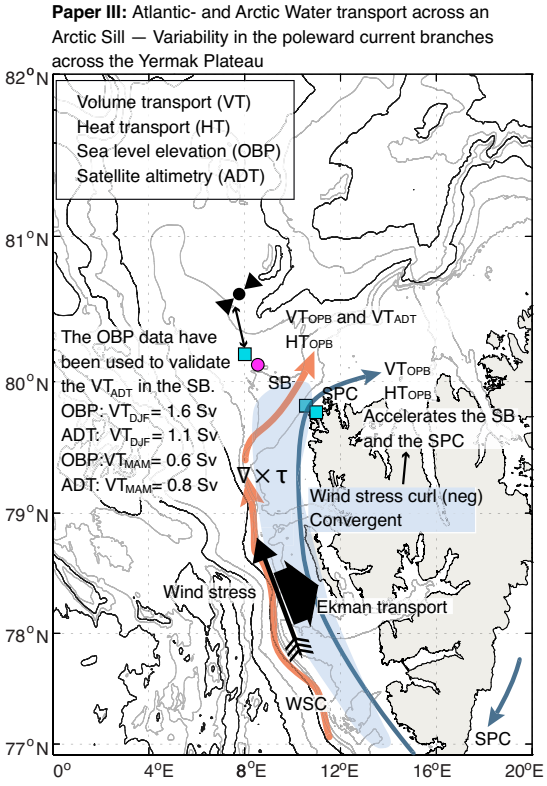

*Figure 4.3: A schematic illustration of the mains findings in **Paper III**.*

Paper IV: **Winter volume and heat transport into the Arctic Ocean from 1994 to 2018 calculated from satellite altimetry.**

Ersdal, E. A., F. Nilsen, R. Skogseth, and E. Falck (Manuscript)

We utilize a 24 year long data record of satellite altimetry to evaluate temporal variations and trends in the volume transport over the Yermak Plateau. Wind stress data in the Fram Strait have been included to gain a better understanding of the atmospheric influence on the branching and inflow of the Atlantic Water on the plateau. Based on the findings in **Paper III**, only the winter months which are assumed to have a well-mixed water column and to be barotropic, have been included. The seasonal mean volume transport has been calculated from December to February (DJF) and March to May

(MAM) in three sections. In addition to the SB and the YPB sections on top of the plateau, a third section upstream of the plateau, the barotropic WSC core near the 79 °N, is included in the study. See the illustration in Figure 4.4. The mean winter vol-

Paper IV: Winter volume and heat transport into the Arctic Ocean from 1994 to 2018 calculated from satellite altimetry

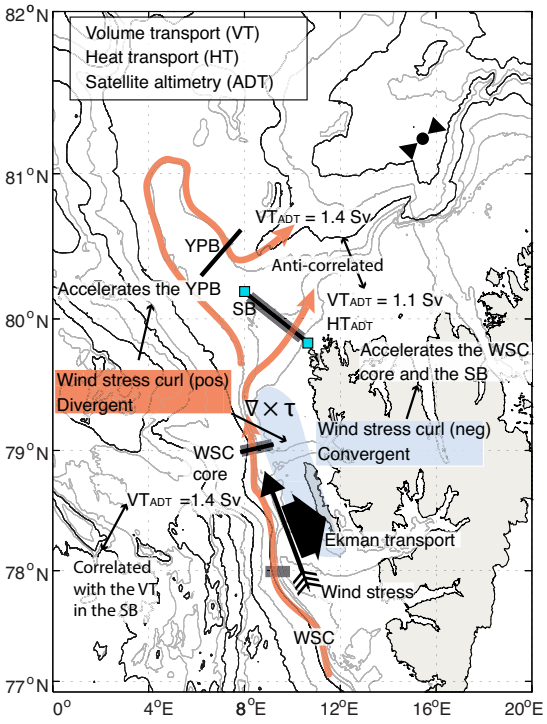

*Figure 4.4: A schematic illustration of the mains findings in **Paper IV**.*

ume transport from 1994 to 2018 was 1.4 Sv in the WSC core, 1.1 Sv in the SB, and 1.4 Sv in the YPB. The comparison with other estimates showed that our values are within the right order of magnitude, but possibly slightly underestimated. **Paper III** compared the volume transport calculated from the ADT and OBP data and found the volume transport from ADT to be underestimated from November to January, and had a small positive bias from February to April. From 1994 to 2018, the volume transport in the WSC core and the SB correlate with each other and with a negative wind stress curl on the West Spitsbergen Shelf (Figure 4.4). A negative wind stress curl on the shelf is linked to coast parallel southerly winds (black arrow), which generate an onshore Ekman transport (wide black arrow). The result is a steepening of the sea surface

tilt that will accelerate the flow in the WSC core and the SB. From March to May, the YPB is anti-correlated with the WSC core and the SB. The YPB also correlated with the northerly coast-parallel winds. Hence, it seems that when the SB slows down, the YPB intensifies.

4.1 Sum up points

1. Based on these model results, we suggest the diurnal tides are enhanced by TTW at the southwestern side the Yermak Plateau. The enhancement of the diurnal tides are most efficient in winter when the WSC is strong.
2. The enhancement of the lower diurnal frequencies O1 and Q1 is linked to a moderate current strength. Hence, O1 and Q1 is probably more frequently enhanced compared to the higher frequencies, K1 and P1.
3. We have observed enhanced low-frequency tides (MSf and Mm) on top of the Yermak Plateau in winter.
4. We suggest the accumulated energy from the enhanced diurnal tides along the slope, which also occur in winter, is nonlineary redistributed to MSf and Mm on top of the plateau.
5. A good understanding of the tidal dynamics over the Yermak Plateau will in time help AVISO/CMEMS to further improve the satellite products north of Svalbard.
6. Satellite altimetry can be used to calculated volume transport on the Svalbard Branch during winter when the water column is homogeneous.
7. The volume transport from satellite altimetry into the Arctic Ocean shows no trend, but the temporal variation is large.
8. The volume transport in the WSC core and the SB correlate, while volume transport in the YPB is anti-correlated with the volume transport in the WSC core and the SB.
9. Southerly coast-parallel wind accelerates the flow in the WSC core and the SB, while northerly coast-parallel winds favours the flow in the YPB.

Chapter 5

Future perspectives

Due to its location at the entrance of the Arctic Ocean, it is crucial to understand the mechanisms driving the inflow of Atlantic Water across the Yermak Plateau. Based on on our findings, it seems like the TTW influence this flow to a larger extent than earlier assumed. For the future, a denser mooring set up along the slope, capturing the structure and temporal variations would provide additional information to refine and improve these analyses. The model results combined with measurement show that the behavior of the TTW changes with the seasons and is especially sensitive to changes in the current strength. A chain of moorings equipped with pressure sensors at the bottom and current meters higher up, will give us the opportunity to measure the structure of the vorticity waves and how it changes with the distance to the shelf. Further, when combining the structure of the wave with the measured along-slope current, we can get an idea of how sensitive the enhancement of the individual diurnal constituents is to current changes.

The model runs showed that the "normal" situation is a negative group velocity along the southwestern slope. This means that the energy will propagate southwards towards the location where the WSC splits into the SB, the YB and the YPB. *von Appen et al.* (2016) used satellite altimetry combined with current meter mooring to map the Eddy kinetic energy in the Fram Strait during summer and winter. They show that in the area where the WSC splits into several branches, the Eddy kinetic energy value has a maximum, especially during winter. The question is then; does this energy influences the branching across the plateau? The existence of TTW further south in the Fram Strait

has been suggested by *Nilsen et al.* (2006), and as the continental shelf continues north of Svalbard, it seems reasonable to assume the same phenomenon are present beyond the plateau. The ocean over the continental shelf north of Svalbard has an observed declining sea ice cover, and another question is whether and how the removal of the sea ice, which acts as a lid and protects the ocean from the wind forcing, will possibly influence and modify these dynamics?

We have suggested the low-frequency tides on top of the plateau receive diurnal tidal energy when the group velocity of the TTW is zero. The total flow set up by MSf and Mm, termed the Nonlinear Yermak Tidal Overflow (NYTO) sends pulses of Atlantic Water across the plateau in winter. These characteristics also fit the Yermak Pass Branch, and therefore it would be interesting to find out whether both the NYTO and the YPB are forced by the TTW with zero group velocity close to the diurnal frequency. Based on these results, one mooring capturing the YPB and a second capturing the NYTO is desirable.

Bibliography

Aagaard, K., A. Foldvik, and S. Hillman (1987), The West Spitsbergen Current: disposition and water mass transformation, *Journal of Geophysical Research: Oceans (1978-2012)*, *92*(C4), 3778–3784, doi:https://doi.org/10.1029/JC092iC04p03778. 2.1.1

Bashmachnikov, I. L., I. E. Kozlov, L. A. Petrenko, N. I. Glock, and C. Wekerle (2020), Eddies in the North Greenland Sea and Fram Strait from satellite altimetry, sar and high-resolution model data, *Journal of Geophysical Research: Oceans*, p. e2019JC015832, doi:https://doi.org/10.1029/2019JC015832. 2.1, 2.1.2

Beszczynska-Möller, A., E. Fahrbach, U. Schauer, and E. Hansen (2012), Variability in Atlantic water temperature and transport at the entrance to the arctic ocean, 19972010, *ICES Journal of Marine Science: Journal du Conseil*, p. fss056, doi:10.1093/icesjms/fss056. 2, 2.1

Bourke, R., A. Weigel, and R. Paquette (1988), The westward turning branch of the West Spitsbergen Current, *Journal of Geophysical Research: Oceans*, *93*(C11), 14,065–14,077, doi:https://doi.org/10.1029/JC093iC11p14065. 2.1

Bringedal, C., T. Eldevik, Ø. Skagseth, M. A. Spall, and S. Østerhus (2018), Structure and forcing of observed exchanges across the Greenland–Scotland Ridge, *Journal of Climate*, *31*(24), 9881–9901, doi:https://doi.org/10.1175/JCLI-D-17-0889.1. 2.1.2

Brink, K. H. (2006), Coastal-trapped waves with finite bottom friction, *Dynamics of Atmospheres and Oceans*, *41*(3), 172–190, doi:https://doi.org/10.1016/j.dynatmoce.2006.05.001. 2.1.1, 3.2

Cartwright, D. (1969), Extraordinary tidal currents near St Kilda, *Nature*, *223*(5209), 928. 2.1.1

Chafik, L., J. Nilsson, Ø. Skagseth, and P. Lundberg (2015), On the flow of Atlantic water and temperature anomalies in the Nordic Seas toward the Arctic Ocean, *Journal of Geophysical Research: Oceans*, *120*(12), 7897–7918, doi:https://doi.org/10.1002/2015JC011012. 2.1.2

Emery, W. J., and R. E. Thomson (2001), *Data analysis methods in physical oceanography*, Elsevier, Amsterdam, 2nd and rev. ed. 3.2

Falck, E. (2019), Arctic Ocean Under Melting Ice (UNDER-ICE), doi:https://doi:10.18712/NSD-NSD2759-V1. 3.1.1

Fer, I., R. Skogseth, and F. Geyer (2010), Internal waves and mixing in the marginal ice zone near the Yermak Plateau, *Journal of Physical Oceanography*, *40*(7), 1613–1630, doi:https://doi.org/10.1175/2010JPO4371.1. 2.1.1, 2.1.1

Fer, I., M. Müller, and A. K. Peterson (2015), Tidal forcing, energetics, and mixing near the Yermak Plateau, doi:https://doi.org/10.5194/os-11-287-2015. 2.1.1, 2.1.1

Foldvik, A., J. H. Middleton, and T. D. Foster (1990), The tides of the southern Weddell Sea, *Deep Sea Research Part A. Oceanographic Research Papers*, *37*(8), 1345–1362, doi:https://doi.org/10.1016/0198-0149(90)90047-Y. 2.1.1

Furevik, T., and A. Foldvik (1996), Stability at M2 critical latitude in the Barents Sea, *Journal of Geophysical Research: Oceans*, *101*(C4), 8823–8837, doi:https://doi.org/10.1029/96JC00081. 2.1.1

Gammelsrød, T., and B. Rudels (1983), Hydrographic and current measurements in the Fram Strait, August 1981, *Polar Research*, *1*(2), 115–126, doi:https://doi.org/10.3402/polar.v1i2.6977. 2.1

Gascard, J.-C., C. Richez, and C. Rouault (1995), New insights on large-scale oceanography in Fram Strait: the West Spitsbergen Current, *Arctic oceanography: marginal ice zones and continental shelves*, pp. 131–182, doi:https://doi.org/10.1029/CE049p0131. 2.1, 2.1, 2.1.1

Graham, R. M., P. Itkin, A. Meyer, A. Sundfjord, G. Spreen, L. H. Smedsrud, G. E. Liston, B. Cheng, L. Cohen, D. Divine, et al. (2019), Winter storms accelerate the

demise of sea ice in the Atlantic sector of the Arctic Ocean, *Scientific reports*, *9*(1), 1–16, doi:https://doi.org/10.1038/s41598-019-45574-5. 2

Hanssen-Bauer, I., E. Førland, H. Hisdal, S. Mayer, A. Sandø, and A. Sorteberg (2019), Climate in Svalbard 2100–a knowledge base for climate adaptation, *Norsk klimaservicesenter (NKSS)/Norwegian Centre for Climate Services (NCCS)*. 2

Hattermann, T., P. E. Isachsen, W.-J. von Appen, J. Albretsen, and A. Sundfjord (2016), Eddy-driven recirculation of Atlantic water in Fram strait, *Geophysical Research Letters*, *43*(7), 3406–3414, doi:https://doi.org/10.1002/2016GL068323. 2.1

Helland-Hansen, B., and F. Nansen (1909), *The Norwegian Sea: its physical oceanography based upon the Norwegian researches 1900-1904*, Det Mallingske Bogtrykkeri. 2.2, 3.2

Hunkins, K. (1986), Anomalous diurnal tidal currents on the yermak plateau, *Journal of Marine Research*, *44*(1), 51–69, doi:https://doi.org/10.1357/002224086788460139. 2.1.1

Huthnance, J. (1978), On coastal trapped waves: Analysis and numerical calculation by inverse iteration, *Journal of Physical Oceanography*, *8*(1), 74–92, doi:https://doi.org/10.1175/1520-0485(1978)008<0074:OCTWAA>2.0.CO;2. 2.1.1

IPCC (2018), *Global Warming of 1.5°C: An IPCC Special Report on the Impacts of Global Warming of 1.5°C Above Pre-industrial Levels and Related Global Greenhouse Gas Emission Pathways, in the Context of Strengthening the Global Response to the Threat of Climate Change, Sustainable Development, and Efforts to Eradicate Poverty*, Intergovernmental Panel on Climate Change. 2

Kantha, L. H., J. S. Stewart, and S. D. Desai (1998), Long-period lunar fortnightly and monthly ocean tides, *Journal of Geophysical Research: Oceans*, *103*(C6), 12,639–12,647, doi:https://doi.org/10.1029/98JC00888. 2.1.1

Koenig, Z., C. Provost, N. Sennéchael, G. Garric, and J.-C. Gascard (2017), The yermak pass branch: A major pathway for the Atlantic water north of Svalbard?, *Journal of Geophysical Research: Oceans*, *122*(12), 9332–9349, doi:https://doi.org/10.1002/2017JC013271. 2.1.1, 2.1.1, 3.2

Kowalik, Z. (1994), Modeling of topographically amplified diurnal tides in the Nordic Seas, *Journal of Physical Oceanography*, *24*(8), 1717–1731, doi:https://doi.org/10.1175/1520-0485(1994)024<1717:MOTADT>2.0.CO;2. 2.1.1

Lavergne, T., A. M. Sørensen, S. Kern, R. Tonboe, D. Notz, S. Aaboe, L. Bell, G. Dybkjær, S. Eastwood, C. Gabarro, et al. (2019), Version 2 of the EUMETSAT OSI SAF and ESA CCI sea-ice concentration climate data records, *Cryosphere*, *13*(1), 49–78, doi:https://doi.org/10.1007/s00382-017-3618-9. 3.1.5

Le Provost, C. (1991), Generation of overtides and compound tides, *Tidal hydrodynamics*, pp. 269–296. 2.1.1

Lilly, J. M., and S. C. Olhede (2009), Higher-order properties of analytic wavelets, *IEEE Transactions on Signal Processing*, *57*(1), 146–160, doi:10.1109/TSP.2008.2007607. 3.2

Manley, T., R. Bourke, and K. Hunkins (1992), Near-surface circulation over the Yermak Plateau in northern Fram Strait, *Journal of Marine Systems*, *3*(1-2), 107–125, doi:https://doi.org/10.1016/0924-7963(92)90033-5. 2.1.1

Marnela, M., B. Rudels, M.-N. Houssais, A. Beszczynska-Möller, and P. Eriksson (2013), Recirculation in the Fram Strait and transports of water in and north of the Fram Strait derived from CTD data, *Ocean Science*, *9*(3), 499, doi:https://doi.org/10.5194/os-9-499-2013. 2.1

Middletton, J. H., T. D. Foster, and A. Foldvik (1987), Diurnal shelf waves in the southern Weddell Sea, *Journal of Physical Oceanography*, *17*(6), 784–791, doi:https://doi.org/10.1175/1520-0485(1987)017<0784:DSWITS>2.0.CO;2. 2.1.1

Morison, J. (1991), Seasonal variations in the West Spitsbergen Current estimated from bottom pressure measurements, *Journal of Geophysical Research: Oceans*, *96*(C10), 18,381–18,395, doi:https://doi.org/10.1029/91JC01916. 3.2

Mork, K. A., and Ø. Skagseth (2010), A quantitative description of the Norwegian Atlantic Current by combining altimetry and hydrography, doi:https://doi.org/10.5194/os-6-901-2010. 2.1.2

Nilsen, F. (2019), Remote Sensing of Ocean Circulation and Environmental Mass Changes (REOCIRC), doi:https://doi.org/10.18712/nsd-nsd2756-v1. 3.1.1

Nilsen, F., B. Gjevik, and U. Schauer (2006), Cooling of the West Spitsbergen Current: Isopycnal diffusion by topographic vorticity waves, *Journal of Geophysical Research: Oceans*, *111*(C8), doi:https://doi.org/10.1029/2005JC002991. 5

Nilsen, J. E. Ø., and F. Nilsen (2007), The Atlantic water flow along the Vøring plateau: detecting frontal structures in oceanic station time series, *Deep Sea Research Part I: Oceanographic Research Papers*, *54*(3), 297–319, doi:https://doi.org/10.1016/j.dsr.2006.12.012. 2.1

Olhede, S. C., and A. T. Walden (2002), Generalized morse wavelets, *IEEE Transactions on Signal Processing*, *50*(11), 2661–2670, doi:10.1109/TSP.2002.804066. 3.2

Onarheim, I. H., L. H. Smedsrud, R. B. Ingvaldsen, and F. Nilsen (2014), Loss of sea ice during winter north of Svalbard, *Tellus A: Dynamic Meteorology and Oceanography*, *66*(1), 23,933, doi:https://doi.org/10.3402/tellusa.v66.23933. 2, 2.1.1

Orvik, K. A., and P. Niiler (2002), Major pathways of Atlantic water in the northern North Atlantic and Nordic Seas toward Arctic, *Geophysical Research Letters*, *29*(19), doi:https://doi.org/10.1029/2002GL015002. 2.1, 2.1

OSISAF (2017), Global Sea Ice Concentration climate data record (SMMR/SSMI/SSMIS), doi:10.15770/EUM_SAF_OSI_0008. 3.1.5

Padman, L., A. J. Plueddemann, R. D. Muench, and R. Pinkel (1992), Diurnal tides near the Yermak Plateau, *Journal of Geophysical Research: Oceans*, *97*(C8), 12,639–12,652, doi:https://doi.org/10.1029/92JC01097. 2.1.1

Parker, B. B. (1991), The relative importance of the various nonlinear mechanisms in a wide range of tidal interactions, *Tidal hydrodynamics*, *237*. 2.1.1

Parker, B. B. (2007), *Tidal Analysis and Prediction*, National Oceanic and Atmospheric Administration National Ocean Service, Silver Spring, Maryland, doi:http://dx.doi.org/10.25607/OBP-191. 2.1.1, 2.1.1

Pawlowicz, R., B. Beardsley, and S. Lentz (2002), Classical tidal harmonic analysis including error estimates in MATLAB using t_tide, *Computers & Geosciences*, *28*(8), 929–937, doi:https://doi.org/10.1016/S0098-3004(02)00013-4. 2.1.1, 3.2

Piechura, J., and W. Walczowski (2009), Warming of the West Spitsbergen Current and sea ice north of Svalbard, *Oceanologia*, *51*(2), 147–164, doi:http://dx.doi.org/10.5697/oc.51-2.147. 2

Polyakov, I. V., A. V. Pnyushkov, M. B. Alkire, I. M. Ashik, T. M. Baumann, E. C. Carmack, I. Goszczko, J. Guthrie, V. V. Ivanov, T. Kanzow, et al. (2017), Greater role for Atlantic inflows on sea-ice loss in the Eurasian Basin of the Arctic Ocean, *Science*, *356*(6335), 285–291, doi:10.1126/science.aai8204. 2

Pörtner, H., D. Roberts, V. Masson-Delmotte, P. Zhai, M. Tignor, E. Poloczanska, K. Mintenbeck, M. Nicolai, A. Okem, J. Petzold, et al. (2019), IPCC Special Report on the Ocean and Cryosphere in a Changing Climate, *IPCC Intergovernmental Panel on Climate Change: Geneva, Switzerland*. 2

Reistad, M., Ø. Breivik, H. Haakenstad, O. J. Aarnes, B. R. Furevik, and J.-R. Bidlot (2011), A high-resolution hindcast of wind and waves for the North Sea, the Norwegian Sea, and the Barents sea, *Journal of Geophysical Research: Oceans*, *116*(C5), doi:https://doi.org/10.1029/2010JC006402. 3.1.4

Reistad, M., H. Haakenstad, B. Furevik, J. Haugen, O. Breivik, and O. Aarnes (2015), Validation of the Norwegian wind and wave hindcast-NORA 10, *Tech. rep.*, MET report. 3.1.4

Rio, M., S. Mulet, and N. Picot (2013), New global Mean Dynamic Topography from a GOCE geoid model, altimeter measurements and oceanographic in-situ data, in *Proceedings of the ESA living planet symposium, Edinburgh*. 2.1.2

Rio, M.-H., S. Mulet, H. Etienne, G. Dibarboure, and P. N. (2018), New CNES-CLS8 mean dynamic topography of the global ocean from altimetry, gravity and ins-situ data. 2.1.2

Rudels, B., R. Meyer, E. Fahrbach, V. Ivanov, S. Østerhus, D. Quadfasel, U. Schauer, V. Tverberg, and R. Woodgate (2000), Water mass distribution in Fram Strait and over

the Yermak Plateau in summer 1997, in *Annales Geophysicae*, vol. 18, pp. 687–705, Springer, doi:https://doi.org/10.1007/s00585-000-0687-5. 2.1.1

Schauer, U., E. Fahrbach, S. Osterhus, and G. Rohardt (2004), Arctic warming through the Fram Strait: Oceanic heat transport from 3 years of measurements, *Journal of Geophysical Research: Oceans*, *109*(C6), doi:https://doi.org/10.1029/2003JC001823. 2

Semper, S., and E. Darelius (2017), Seasonal resonance of diurnal coastal trapped waves in the southern Weddell Sea, Antarctica, *Ocean Science*, *13*(1), 77, doi:https://doi.org/10.5194/os-13-77-2017. 2.1.1

Sirevaag, A., and I. Fer (2009), Early spring oceanic heat fluxes and mixing observed from drift stations north of svalbard, *Journal of physical oceanography*, *39*(12), 3049–3069, doi:https://doi.org/10.1175/2009JPO4172.1. 2.1.1

Skarðhamar, J., Ø. Skagseth, and J. Albretsen (2015), Diurnal tides on the barents sea continental slope, *Deep Sea Research Part I: Oceanographic Research Papers*, *97*, 40–51, doi:https://doi.org/10.1016/j.dsr.2014.11.008. 2.1.1

Skogseth, R., P. Ellingsen, J. Berge, F. Cottier, S. Falk-Petersen, B. Ivanov, and A. Vader (2019), UNIShydrographic database, doi:https://doi.org/10.21334/unis-hydrography. 3.1.3

Skogseth, R., L. L. Olivier, F. Nilsen, E. Falck, N. Fraser, V. Tverberg, A. Ledang, A. Vader, M. Jonassen, J. Søreide, et al. (2020), Variability and decadal trends in the Isfjorden (Svalbard) ocean climate and circulation-an indicator for climate change in the European Arctic, *Progress in Oceanography*, p. 102394, doi:https://doi.org/10.1016/j.pocean.2020.102394. 2, 3.1.3

Teigen, S. H., F. Nilsen, and B. Gjevik (2010), Barotropic instability in the West Spitsbergen Current, *Journal of Geophysical Research: Oceans*, *115*(C7), doi:https://doi.org/10.1029/2009JC005996. 2.1, 2.1

Teigen, S. H., F. Nilsen, R. Skogseth, B. Gjevik, and A. Beszczynska-Möller (2011), Baroclinic instability in the West Spitsbergen Current, *Journal of Geophysical Research: Oceans*, *116*(C7), doi:https://doi.org/10.1029/2011JC006974. 2.1, 2.1

von Appen, W.-J., U. Schauer, T. Hattermann, and A. Beszczynska-Möller (2016), Seasonal cycle of mesoscale instability of the west spitsbergen current, *Journal of Physical Oceanography*, *46*(4), 1231–1254, doi:https://doi.org/10.1175/JPO-D-15-0184.1. 2.1, 2.1.2, 5

Walczowski, W., and J. Piechura (2006), New evidence of warming propagating toward the Arctic Ocean, *Geophysical Research Letters*, *33*(12), doi:https://doi.org/10.1029/2006GL025872. 2.1

Wickström, S., M. Jonassen, T. Vihma, and P. Uotila (2019), Trends in cyclones in the high-latitude North Atlantic during 1979–2016, *Quarterly Journal of the Royal Meteorological Society*, doi:https://doi.org/10.1002/qj.3707. 2

Wuncsh, C. (1967), The long-period tides, *Reviews of Geophysics*, *5*(4), doi:https://doi.org/10.1029/RG005i004p00447. 2.1.1

Chapter 6

Scientific results

I

Paper I

Topographically trapped waves along an Arctic continental shelf in reso-nance with diurnal tidal frequencies

Ersdal, E. A. and F. Nilsen (2020, in prep.)

Submitted to JGR-Ocean in Sept 2019 and re-submitted August 2020

Paper II

On nonlinearly enhanced low-frequency tides over the Yermak Plateau

Ersdal, E. A., F. Nilsen, and T. Gammelsrød (2020, in prep.)

Submitted to JGR-Ocean in Sept 2019

II

Paper III

Atlantic- and Arctic Water transport across the Arctic Sill - Variability in the poleward current branches across the Yermak Plateau

Nilsen, F., E. A. Ersdal, and R. Skogseth (2020, in prep.)

Manuscript

III

Paper IV

Winter volume and heat transport into the Arctic Ocean from 1994 to 2018 calculated from satellite altimetry

Ersdal, E. A., F. Nilsen, R. Skogseth, and E. Falck (2020, in prep.)

Manuscript

IV

Graphic design: Communication Division, UiB / Print: Skipnes Kommunikasjon AS

uib.no

ISBN: 9788230842744 (print)
9788230843826 (PDF)